$CeNi_x$ Alloys as Catalysts for Ammonia Synthesis: Insights on Ni−CeN Surface Layer Formation and Its Impact

Javier Arroyo-Caire, Yihao Jiang, Manuel Antonio Diaz-Perez, Mayra Anabel Lara-Angulo, Masayoshi Miyazaki, Juan Serrano-Ruiz,* Masaaki Kitano,* and Hideo Hosono*

ABSTRACT: Ammonia, which is widely used for the production of fertilizers, is becoming increasingly important as a hydrogen-containing energy vector. Typically, the ammonia synthesis activity of non-noble cheap metal-based catalysts (e.g., Ni) is well below that of ruthenium or cobalt. In this work, we unveil the performance of bulk $CeNi_x$ alloys as compact bimetallic catalysts for ammonia synthesis. The spontaneous formation of a crystalline CeN surface layer was responsible for the higher activity of $CeNi_2$ over $CeNi_5$ (1. 012and 0. 067mmol g^{-1} h^{-1}, respectively) at 400 °C and 0.9 MPa. The CeN layer was key since it served as a second active center for nitrogen dissociation, enhancing the ammonia synthesis rate to levels comparable to other rare earth-based alloys. Significant differences in the global kinetic mechanism were also found: $CeNi_2$ showed significantly lower apparent activation energies than $CeNi_5$ (55.3 vs 79.5 kJ mol^{-1}, respectively). Furthermore, $CeNi_2$ showed synthesis rates 1 order of magnitude higher than pure bulk CeN, thereby stressing the key role of Ni as an additional center for hydrogen and hydrogen-containing species (NH_x) activation. We also demonstrated that the chemical state of cerium (oxide vs nitride) is key for enhancing the ammonia synthesis reaction. We found that Ce is required to be in the form of nitride for enhancing the activity of CeNi2, as revealed by the poor kinetic behavior (high activation energy, strong hydrogen poisoning, and poor affinity toward NHx species) and low synthesis rates found for a nanopowder Ni/CeO2 catalyst.

KEYWORDS: nickel, CeNix alloys, CeN surface layer, second active center, non-noble metal-based catalysts

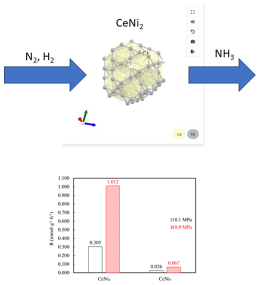

1. INTRODUCTION

Ammonia (NH_3) has recently gained attention as a chemical platform, not only for its increasing use in the fertilizer industry[1] but also due to its potential role as an energy carrier, owing to its large hydrogen content (18 wt %).[2−5] The Haber−Bosch (HB) process, traditionally used to produce ammonia, is highly energy-consuming since harsh operating conditions (i.e., 20−40 MPa and 400−600 °C) are required to achieve the dissociation of a very stable nitrogen molecule (N_2).[6]

In this context, strong efforts have been made to develop more efficient catalysts able to achieve reasonable ammonia synthesis performance at milder conditions.[3,7−11] This approach is particularly interesting for integrating NH_3 synthesis with renewable hydrogen production via water electrolysis, thereby paving the way for a new paradigmatic small-scale distributed green ammonia production.[12] 3d transition metals (TMs), such as ruthenium (Ru), have demonstrated high ammonia synthesis activities at milder conditions,[7,8] owing to its optimum nitrogen absorption energy.[13] However, despite its superior activity, the high cost of Ru hinders its widespread use at the industrial scale. Thus, the design of non-noble-metal-based catalysts for ammonia production is highly desirable. However, when selecting non-noble metals for this application, it is necessary to consider their affinity toward nitrogen (i.e., adsorption energy) since the adsorption and subsequent dissociation of N_2 is a key step in ammonia synthesis.[14] Some non-noble metals such as Ni present very low affinity toward N_2. This limitation has recently been overcome by using active supports with the ability to activate and dissociate N_2, such as hydrides (e.g., LiH[15]) or rare-earth (RE) nitrides (RE = Ce, La, Y).[16] While hydrides allow N_2 dissociation by promoting simultaneous electron and H^- transfer processes, nitrides promote N_2 adsorption and activation by providing nitrogen vacancy (N_V) surface sites.

RE elements have attracted significant attention in the field of ammonia synthesis at mild conditions.[17] Their versatile chemical nature allows them to generate different active centers, thereby facilitating the dispersion of TMs on their surface. In the case of RE oxides, the high reducibility of these materials results in the formation of surface oxygen vacancies upon reduction, promoting the so-called strong metal−support interaction (SMSI). The formation of these oxygen vacancies improves the dispersion of the TM while promoting electron transfer

processes toward the metal, thereby facilitating the activation and dissociation of the N_2 molecule.[17,18] This strategy has demonstrated to be useful for metals with optimum nitrogen absorption energy, such as Ru[19,20] or Co.[21] RE hydrides and oxyhydrides have shown higher activities compared to RE oxides since the highly mobile H^- further enhances the electron donation process.[22,23] In general, the use of a suitable material as a secondary active center has been demonstrated to boost the activity of TMs with optimum nitrogen absorption energies.

In the case of metals with low affinity to nitrogen, such as Ni, RE oxides are less efficient and new strategies are required.[8] In this sense, Ni has recently demonstrated to have a superior performance when promoted with RE nitrides[16] since N_V sites can activate H_2 and, particularly, N_2. Among the RE nitrides, CeN has shown a superior performance for ammonia synthesis compared to LaN and YN because of its lower N_V formation energy (i.e., E_{N_V} = 1.3 eV). Bulk 5 wt % Ni/CeN has shown an outstanding ammonia synthesis activity of 3100 μmol g^{-1} h^{-1} at 400 °C and 1 bar.[16]

Intermetallic RETM compounds are currently gaining attention as ammonia synthesis catalysts[24−29] since the close interaction between RE and TM promotes N_2 dissociation efficiently. $RETM_x$ alloys (x = 2, 3, 5) have been found useful for several applications,[30,31] particularly as hydrogen storage materials,[32−35] in virtue of their ability to reversibly form hydrogenated complexes. This ability of $RETM_x$ intermetallics is particularly interesting for ammonia synthesis applications. Recently, $LaNi_5$ alloy nanoparticles (NPs) have shown outstanding ammonia synthesis activities (4500 μmol g^{-1} h^{-1} at 400 °C and 1 bar) with apparent activation energies as low as 53.8 kJ mol^{-1}. $LaNi_5$ has clearly outperformed other Ni-based materials, showing activities in the range (or even slightly higher) of those of Ru-based intermetallic compounds. The superior performance of $LaNi_5$ has been ascribed to the formation of a Ni−LaN surface layer upon reaction, resulting in a self-organized core (Ni)−shell (LaN) material.[36] The formation of secondary or intermediate phases has received growing interest in the field of ammonia synthesis and catalyst design. TM or primary phase encapsulation has demonstrated to lead to a dramatical increase in the ammonia synthesis performance of original materials, principally as a result of the formation of secondary active phases as in the case of $LaNi_5$[36] or for conventional TM/support materials, such as Co/BaO-La_2O_3[37] In this case, the formation of surface nanolayers encapsulating the TM is reported to enhance the electron transfer, further enhancing ammonia synthesis as compared to the original catalyst.

In this work, we provide new insights into the performance of bulk $CeNi_x$ (x = 2, 5) alloys. Remarkably, we found $CeNi_2$ alloys to outperform bulk $LaNi_5$ by 20% in terms of the ammonia production rate at similar conditions. We also demonstrated that the performance of $CeNi_x$ alloys relies on the formation of a CeN surface layer over the fresh catalyst and analyzed the relationship between the formation of this CeN phase and the ammonia synthesis rate. We found that the $CeNi_2$ performance and kinetic mechanism clearly exceed those of pure bulk CeN, with Ni playing a crucial role as a second active center for hydrogen dissociation and hydrogenation of the adsorbed nitrogen species. Furthermore, the importance of the chemical state of cerium in the nitride phase was highlighted. The $CeNi_2$ alloy catalyst showed significantly higher ammonia synthesis rates and lower apparent activation energies than did a regular Ni/CeO_2 catalyst. Ni/CeO_2 also showed negative and zero reaction orders toward hydrogen and ammonia, respectively, revealing a less efficient global kinetic mechanism as compared to the $CeNi_2$ alloy catalyst.

2. EXPERIMENTAL SECTION

2.1. Catalyst Preparation. $CeNi_x$ ingots were prepared by arc melting of specific mixtures (Ni/Ce molar ratio x = 2:5) of pure elemental Ce shots (99.9%, Rare Metallic Co.) and pellets of Ni powder (Kojundo Chemical Laboratory Co.), while bulk $CeNi_x$ powders were obtained by crushing the as-received ingots using an agate mortar, as reported previously.[36]

Bulk CeN samples were collected from previous batches and synthesized following a hydrogenation + nitridation process from pure Ce shots, as reported previously.[16]

Ni/CeO_2 NPs were prepared by loading Ni (20 wt %) over pure CeO_2 NPs through a solid-state reaction of nickelocene (>98.0%, Tokyo Chemical Industry Co.) and CeO_2 (Sigma-Aldrich), mixed in an agate mortar, followed by a reduction stage, as previously reported.[16]

Since Ce shots, nitrides, and alloys are air- and/or moisture-sensitive, material handling, crushing, and solid-state reaction procedures were all conducted inside an Ar-filled glovebox.

2.2. Ammonia Synthesis Tests. Catalytic reactions were carried out in a stainless-steel fixed-bed reactor under a stoichiometric N_2/H_2 (1:3) flow of 60 mL min^{-1}. A WHSV of 36000 mL g^{-1} h^{-1} was settled, so 0.1 g of the catalyst bed was used. The ammonia produced was monitored under steady-state conditions of temperature (340−400 °C) and pressure (0.1−0.9 MPa). A thermocouple was directly placed into the catalyst in order to minimize temperature errors. The ammonia produced was trapped in a 5 mM aqueous sulfuric acid solution, and the concentration of NH^{4+} ions was determined using an ion chromatograph (Prominence, Shimadzu) equipped with an electrical conductivity detector. Ar gas was used as an inert diluent gas for measuring the N_2 and H_2 reaction orders to ensure a total flow of 60 mL min^{-1} when changing the flow rate of N_2 and H_2.

2.3. Characterization. Crystal structures were analyzed using X-ray diffraction (XRD; D2 Phaser, Bruker) with Cu Kα radiation (λ = 0.15418 nm). All of the samples were placed in Ar-filled capsules to avoid air oxidation. Nitrogen adsorption measurements (BELSORP-mini II, BEL) were used to obtain the Brunauer−Emmet−Teller (BET) surface areas of the samples. X-ray photoelectron spectroscopy (XPS) (KRATOS ULTRA2, Shimadzu) analyses were carried out using Mg Kα radiation at <10^{-6} Pa, applying 8 kV voltage to the X-ray source. A sample holder was transported inside an ultrahigh vacuum (UHV) apparatus from an Ar-filled glovebox to avoid air contamination. Carbon 1s peak (binding energy = 284.6 eV) was used as a reference for sample measurements. Temperature-programmed desorption (TPD) analyses of hydrogen (m/z = 2), nitrogen (m/z = 28), and ammonia (m/z = 17) were performed to measure the amount of adsorbed gases in all samples using a BELCAT-A (BEL) instrument. Typically, 0.03−0.05 g of the sample was placed in a quartz glass cell inside an Ar-filled glovebox before the measurements. This cell was heated (10 °C min^{-1}) under an Ar stream (30 mL min^{-1}) and the concentrations of N_2, H_2, and NH_3 were monitored by a thermal conductivity detector (TCD) and a mass spectrometer (Bell Mass, BEL).

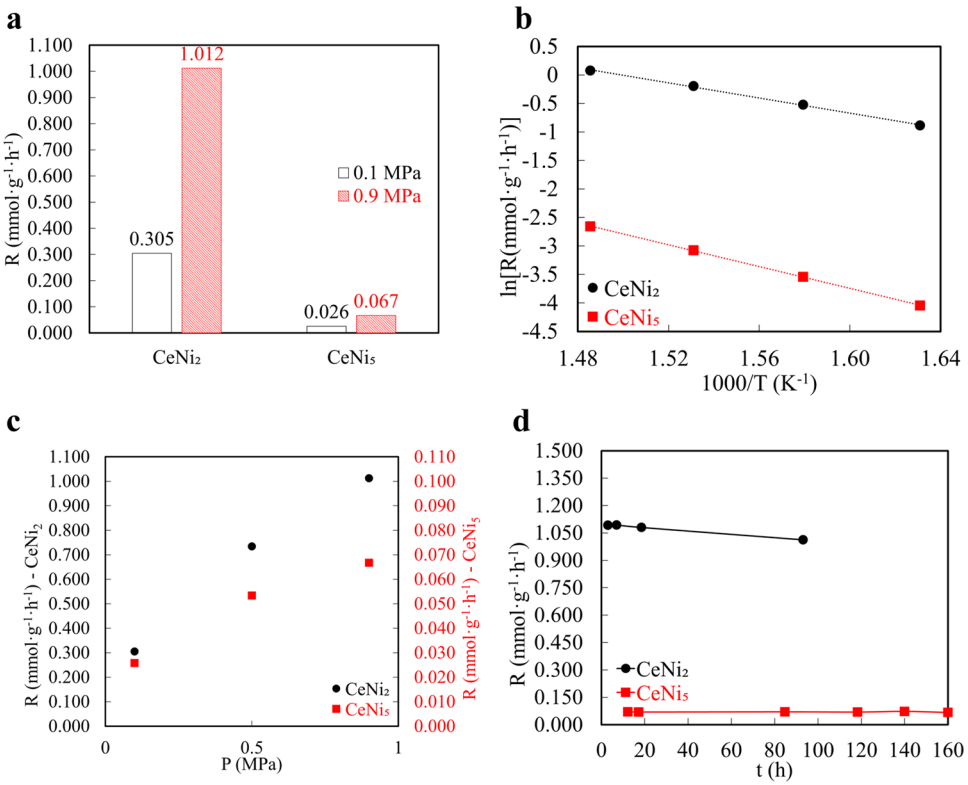

Figure 1. $CeNi_x$ alloy kinetic analysis results. (a) Ammonia synthesis rates at 0.1 and 0.9 MPa. Conditions: 400 °C, 36,000 mL g^{-1} h^{-1}, N_2/H_2 = 1:3, 0.1 g of the catalyst. (b) Arrhenius plots for ammonia synthesis at 0.9 MPa. (c) Ammonia synthesis rate as a function of pressure at 400 °C. (d) Time course of the ammonia synthesis at 0.9 MPa and 400 °C.

3. RESULTS AND DISCUSSION

3.1. Ammonia Synthesis Performance of $CeNi_x$. To study the catalytic behavior of Ce−Ni alloys, two catalysts with different Ni/Ce molar ratios were synthesized, as described in the Section 2. Kinetic experiments were conducted for both bulk $CeNi_2$ and bulk $CeNi_5$ to compare their performance. Prior to these kinetic tests, a preactivation stage was carried out for both catalysts during 2 h, at 500 °C, under a total gas flow (N_2/H_2 = 1:3) of 60 mL min^{-1}, at a pressure of 0.1 MPa, to make sure that the catalyst is homogeneously formed. A layer of CeN emerges during the activation stage for $CeNi_2$, and its formation process and impact on the ammonia synthesis are described in Section 3.2. Figure 1a shows the performances of $CeNi_2$ and $CeNi_5$ at 0.1 and 0.9 MPa, respectively. $CeNi_2$ showed ammonia production rates several orders of magnitude higher than $CeNi_5$ under similar conditions. Interestingly, $CeNi_2$ showed ammonia production rates 20% higher than previously reported bulk $LaNi_5$ (0.305 vs 0.250 mmol g^{-1} h^{-1}) at the same conditions (400 °C, 0.1 MPa, WHSV of 36,000 mL g^{-1} h^{-1}, N_2/H_2 = 1:3).[36]

With the aim to gain insight into the different kinetic behavior of $CeNi_2$ and $CeNi_5$, the Arrhenius plots for $CeNi_2$ and $CeNi_5$ were built (Figure 1b). Both alloys showed an appreciable difference, not only in terms of catalytic activity but also regarding the kinetic mechanism. Arrhenius plots revealed an apparent activation energy of 55.3 kJ mol^{-1} for $CeNi_2$, significantly lower than those of well-known Ru-based catalysts (80−150 kJ mol^{-1})[7] and lower than that of $CeNi_5$ (79.5 kJ mol^{-1}). Since traditional Ru-based catalysts are typically controlled by the nitrogen dissociation step, these results seem to indicate that the rate-determining step (RDS) for $CeNi_2$ is not N_2 dissociation, and it tends to shift toward the formation of NH_x species.[38] This is further confirmed by the reaction orders (Table 1), the experiments of which were driven at 0.9 MPa. The procedure for the reaction order calculation is detailed in the Supporting Information, Section S1. A nitrogen reaction order (α) closer to unity for $CeNi_5$ reveals a higher predominance of N_2 dissociation in the global kinetic scheme, as reported previously.[7,23,39,40] The positive hydrogen reaction orders (β) obtained for both $CeNi_2$ and $CeNi_5$ revealed the absence of hydrogen poisoning issues on these alloys.[7,39,41,42] $CeNi_2$ showed a significantly higher hydrogen reaction order than $CeNi_5$, thereby revealing hydrogen adsorption and dissociation processes to be much more relevant in the reaction mechanism on the former alloy.[7] The positive β values for both $CeNi_2$ and $CeNi_5$ were reflected in a positive and almost linear effect of the pressure on the reaction rate (Figure 1c), although the positive effect was more noticeable for the $CeNi_2$ alloy. The slopes of plots in Figure 1c, calculated as variations of the ammonia synthesis rate with pressure divided by the ammonia synthesis rate at 0.1 MPa, were found to be 2.9 and 2.0 MPa^{-1} for $CeNi_2$

Table 1. Kinetic Parameters of $CeNi_x$ Alloys in the Ammonia Synthesis Reaction[a]

catalyst	E_A (kJ mol^{-1})	α (N_2)	β (H_2)	γ (NH_3)
$CeNi_2$	55.3	0.663	1.089	−0.725
$CeNi_5$	79.5	0.884	0.633	−0.690

[a] E_A: apparent activation energy, α: nitrogen reaction order, β: hydrogen reaction order, γ: ammonia reaction order. Experimental conditions: 400 °C, 36,000 mL g^{-1} h^{-1}, N_2/H_2 = 1:3, 0.1 g of the catalyst.

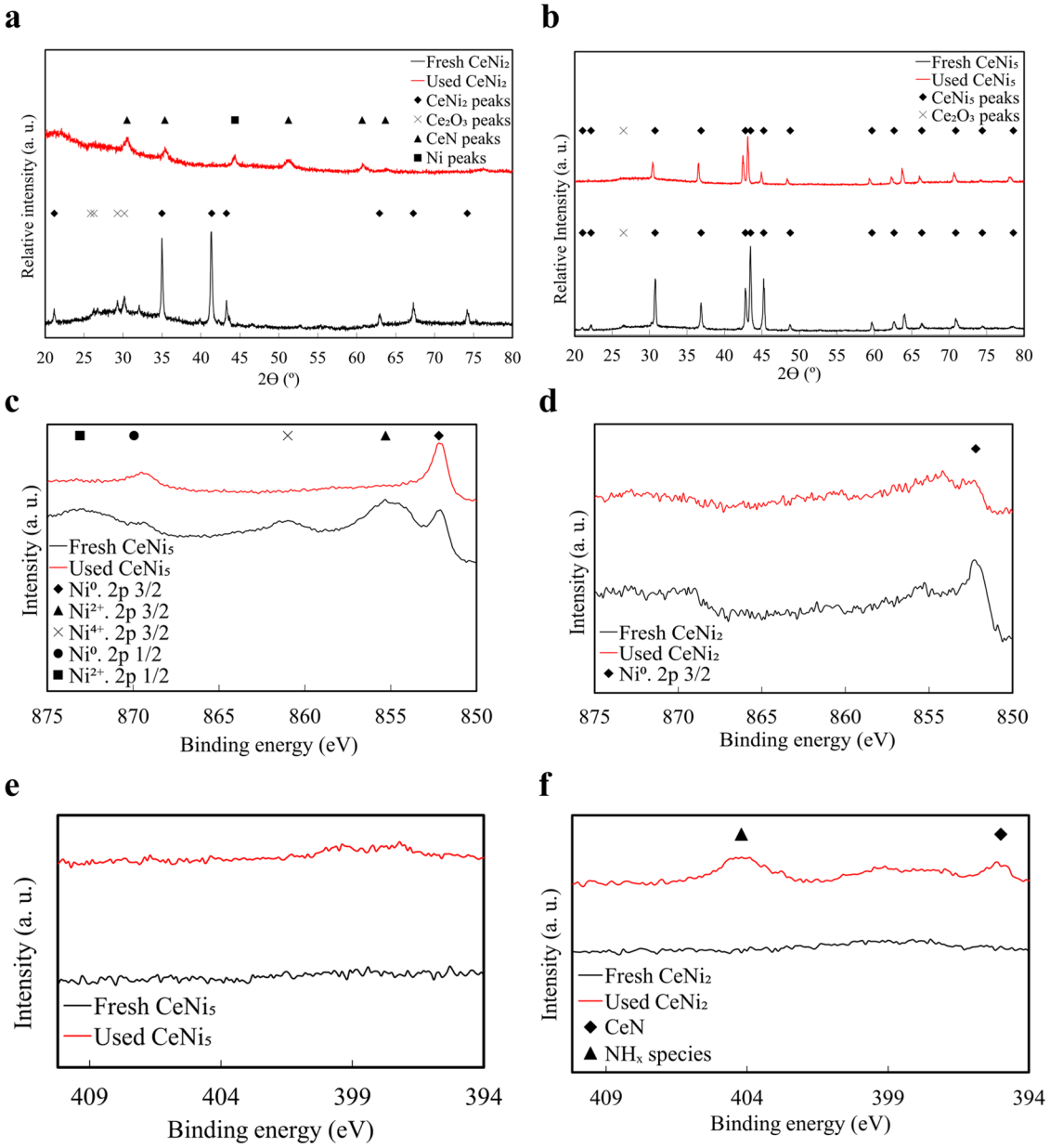

Figure 2. Characterization of $CeNi_x$ alloys. (a) XRD crystal structure of fresh and used $CeNi_2$. (b) XRD crystal structures of fresh and used $CeNi_5$. (c) Ni 2p XPS patterns of fresh and used $CeNi_5$. (d) Ni 2p XPS patterns of fresh and used $CeNi_2$. (e) N 1s XPS patterns of fresh and used $CeNi_5$. (f) N 1s XPS patterns of fresh and used $CeNi_2$.

and $CeNi_5$, respectively. The different β values for both catalysts can account for this different effect of pressure on the reaction rate.[7] For its part, ammonia reaction orders (γ) were very negative and nearly similar for both alloy catalysts.

Both $CeNi_2$ and $CeNi_5$ remained highly stable after 3 h on stream (Figure 1d). $CeNi_2$ (8% ammonia synthesis rate loss after 90 h on stream) and $CeNi_5$ (6% activity loss after 160 h on stream) were slightly deactivated with time. Therefore, total reaction times of 90 and 160 h were counted for $CeNi_2$ and $CeNi_5$, respectively.

To understand the differences between $CeNi_2$ and $CeNi_5$, BET surface analyses were carried out. Both catalysts showed similar surface areas (Table S1), thereby ruling out some effect of this parameter on the higher performance of $CeNi_2$ as compared to $CeNi_5$. Further characterization was required to understand the different behavior of both alloys. Crystal structures were determined by means of X-ray diffraction (XRD) analyses. XRD patterns of $CeNi_2$ and $CeNi_5$ are shown in Figure 2a,2b, respectively. From now on, note that all as-received catalysts, before the preactivation stage, will be defined as "fresh", while after-reaction materials will be named as "used".

As observed, crystal structures ascribed to $CeNi_2$ (Figure 2a) and $CeNi_5$ (Figure 2b) were confirmed for fresh samples (black lines), with minor peaks corresponding to Ce_2O_3 as a result of slight oxidation due to residual exposure to air inside the glovebox. After the reaction (red lines), $CeNi_5$ preserved its crystal structure, with slight angle shifting of the major $CeNi_5$ peaks. However, a change in crystal structure was observed for $CeNi_2$ after the reaction, showing a transformation from a nearly pure $CeNi_2$ phase to pure CeN, with one additional peak corresponding to Ni metal. Remarkably, no formation of the CeN phase was observed for CeNi5 after the reaction. As it will

be discussed later in Section 3.2, the formation of this crystalline phase of CeN can explain the outstanding performance of $CeNi_2$ as compared to $CeNi_5$.

The formation of nitrogen vacancies has been demonstrated to promote efficient N_2 dissociation over a Ni/CeN catalyst and in the absence of metal (pure CeN phase) in previous studies.[16] Bulk Ni/CeN (i.e., specific surface area of around 2 m^2 g^{-1}) showed a very low apparent activation energy (53.4 kJ mol^{-1}), which is very similar to that measured herein for $CeNi_2$ (55.3 kJ mol^{-1}, Table 1), which strongly supports the idea that the CeN phase plays a key role in the reaction by providing a second active center (i.e., nitrogen vacancies) for nitrogen dissociation. CeN generates nitrogen vacancies more easily (formation energy: 1.39 eV) than other nitrides such as LaN (1.72 eV),[16] which can explain the superior performance of bulk $CeNi_2$ versus bulk $LaNi_5$ since a self-organized nitride surface layer is generated spontaneously for both catalysts. In terms of ammonia synthesis activity and the complete kinetic mechanism, $CeNi_2$ and previously reported Ni/CeN cannot be easily contrasted since chemical composition and particle structure configuration are different for both materials. Nevertheless, the similarity in their apparent activation energy values leads to a switch of the RDS toward the formation of NH_x species for both materials, as aforementioned.

To further investigate CeN formation and the surface composition of both $CeNi_2$ and $CeNi_5$, X-ray photoelectron spectroscopy (XPS) experiments were conducted. As shown in Figure 2c, regarding Ni 2p XPS patterns, two positively charged Ni species (Ni^{2+} and Ni^{4+}) and metal Ni^0 were detected for the fresh $CeNi_5$ sample (black line). However, only Ni^0 species were detected for the used sample, revealing a reduction of metal on the $CeNi_5$ surface during the preactivation and initial reaction stages. In contrast, only Ni^0 species was detected for the fresh $CeNi_2$ sample (Figure 2d, black line). As in the case of $CeNi_5$, one could expect a clear presence of Ni^0 after the reaction for $CeNi_2$. However, metallic Ni was practically negligible for used $CeNi_2$ (Figure 2d, red line). This could indicate that a layer of CeN was formed in this catalyst during the reaction, encapsulating the Ni species. Similar conclusions can be obtained by analyzing the Ni 3p pattern (Figure S2c).

To confirm the formation of a surface nitride over the $CeNi_2$ catalyst, the N 1s XPS signals were analyzed (Figure 2e,f). No nitrogen species were detected over the used $CeNi_5$, which suggests that the formation of the CeN phase is negligible. However, two nitrogen peaks were clearly observed for $CeNi_2$ (Figure 2f). The peak at 394.8 eV was attributed to N^{3-} from CeN, in line with the only peak detected from the N 1s XPS pattern of bulk CeN (Figure S2e). Apart from this peak, $CeNi_2$ also showed an XPS peak at very high binding energies (404.0 eV), which can be ascribed to nitrogen species with high electron charge, most of them in the form of nitrates. Despite there are barely reported negatively charged N species around this binding energy, XPS N 1s patterns from previous investigations on Co−Cr−Mo alloys with implanted nitrogen ions[43] revealed the presence of nitrogen in the form of NH_3 or NH_4 over the alloy surface at higher binding energies (ca. 400 eV) than nitride N^{3-} species (ca. 397 eV). These findings suggest that the peak at 404.0 eV observed for the used $CeNi_2$ may correspond to species with a less negative charge than the N^{3-} species peak, i.e., N^{2-} or N^-, which could reveal the presence of NH_x species on the surface of used $CeNi_2$.

In summary, experimental characterization reveals that fresh $CeNi_2$ turns into a catalyst made of a crystalline phase of Ni and CeN (Figure 2a), in which a surface layer of CeN is spontaneously formed (Figure 2f), while the $CeNi_5$ structure remains unaltered.

3.2. Role of the CeN Surface Layer Formation: Temperature Effect. To further confirm the role of the CeN layer formation over the $CeNi_2$ alloy, a series of experimental runs were conducted. In these runs, 0.1 g of fresh $CeNi_2$ was loaded into the reactor and heated at a certain temperature (4 °C min^{-1}) under a total gas pressure (N_2/H_2 = 1:3) of 0.1 MPa and a WHSV of 36,000 mL g^{-1} h^{-1}. Once the set point temperature was reached for every run, the operating pressure was increased to 0.9 MPa and an activation stage of 5 h was performed for promoting CeN layer formation. Once this time lapse was over, the ammonia synthesis rate was measured. After each run, XRD analyses were conducted. The operating temperatures for every run are shown in Table 2 An additional preactivation stage, similar to that conducted in experiments from Section 3.1 (2 h at 500 °C), was carried out in run 8.

Table 2. Temperature Conditions of the Different Runs for CeN Surface Layer Formation Experiments

run	temperature (°C)	additional preactivation stage
1	100	no
2	200	
3	250	
4	300	
5	350	
6	380	
7	400	
8	400	500 °C for 2 h

The evolution of the crystal structure with the run number is shown in Figure 3a. Remarkably, modifications of the crystal structure of the original fresh $CeNi_2$ sample were found to take place at temperatures as low as 100 °C. Interestingly, during this transformation process, a completely amorphous phase was observed at temperatures below 380 °C (runs 1−5), while an incipient crystalline phase is only visible at 380 and 400 °C (runs 6−7). Thus, the crystal structure of the fresh catalyst was self-organized, turning eventually into a crystalline CeN surface layer after 500 °C pretreatment (run 8). Remarkably, this pretreatment is similar to that used for the experiments shown in Section 3.1, which highlights the relevance of this preactivation stage. Similar results were obtained previously for $LaNi_5$,[36] in which a self-organized LaN−Ni structure was spontaneously formed over the original alloy surface, increasing the ammonia synthesis performance by providing the LaN second phase with activity toward N_2 dissociation.

The ammonia synthesis rates for every run are listed in Figure 3b. The activities remained below the detection limit up to 350 °C. At 380 and 400 °C (runs 6 and 7), the CeN crystalline layer was not completely formed (Figure 3a) and ammonia synthesis rates were 1 order of magnitude lower than those reported in Section 3.1. The activation pretreatment at 500 °C (run 8) led to the complete formation of a crystalline surface CeN phase over the $CeNi_2$ catalysts, which was accompanied by a 4-fold increase of the reaction rate versus run 7 despite being carried out at the same temperature (Figure 3b). These results clearly demonstrate that the CeN phase generated upon pretreatment at 500 °C has a crucial role in the ammonia synthesis performance of $CeNi_2$.

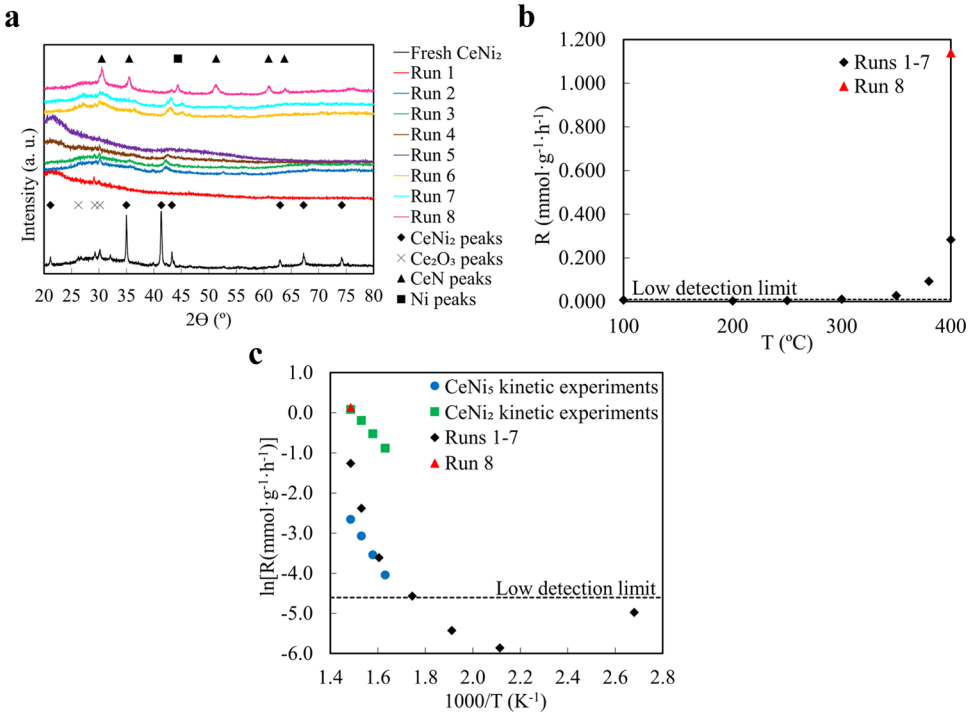

Figure 3. CeN formation layer analysis results. (a) XRD crystal structure of runs 1−8 for $CeNi_2$. (b) Ammonia synthesis rate of runs 1−8 of $CeNi_2$ at onset temperatures. (c) Arrhenius plots of runs 1−8 of $CeNi_2$, compared to $CeNi_x$ plots from kinetic experiments done in Section 3.1 (reaction conditions: 0.1 g of the catalyst, N_2/H_2 = 1:3, 36,000 mL g^{-1} h^{-1}, 0.9 MPa).

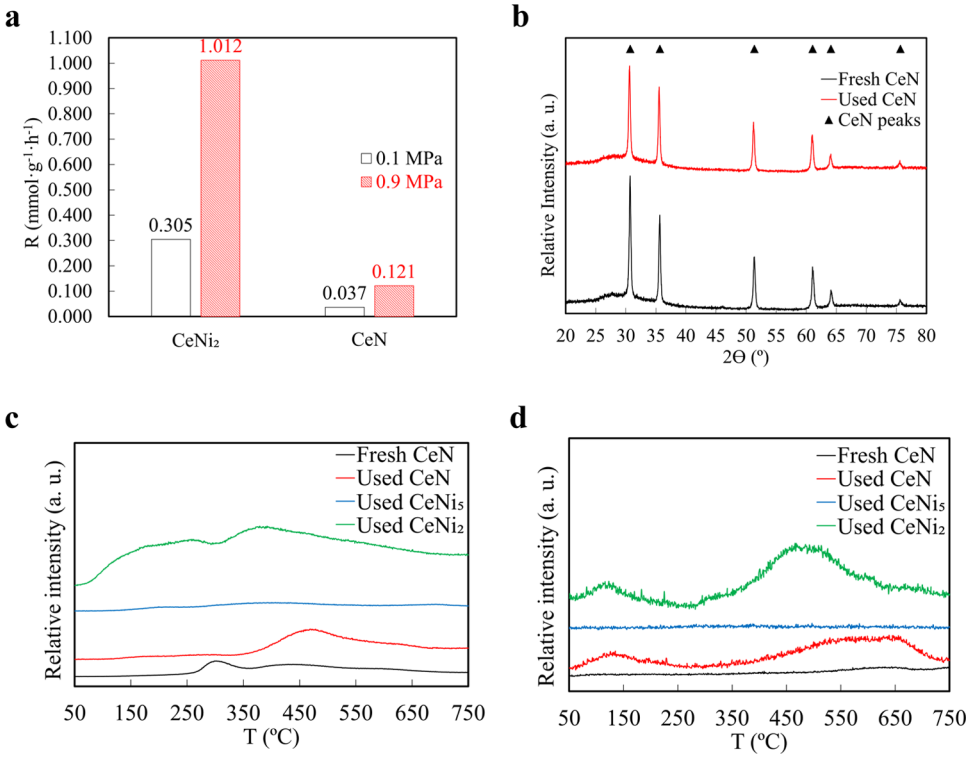

Figure 4. Bulk CeN results and characterization and TPD profiles. (a) Ammonia synthesis rates of $CeNi_2$ (red) and bulk CeN (black) at 0.1 and 0.9 MPa, 400 °C, 36000 mL g^{-1} h^{-1}, N_2/H_2 = 1:3, and 0.1 g of the catalyst. (b) XRD crystal structure of fresh and used CeN. (c) H_2 TPD profiles of fresh and used CeN and $CeNi_x$ alloys. (d) N_2 TPD profiles of fresh and used CeN and $CeNi_x$ alloys.

The ammonia synthesis rates from runs 1−7 were compared with those from previous kinetic experiments of $CeNi_2$ and $CeNi_5$ in the form of Arrhenius plots (Figure 3c). As expected, the rates from run 8 were similar to those obtained for $CeNi_2$ at 400 °C (Section 3.1) since both experiments were performed under similar operating conditions and with the same preactivation stage at 500 °C. At 350−380 °C (runs 6 and 7), the synthesis rates were close to those obtained for $CeNi_5$,

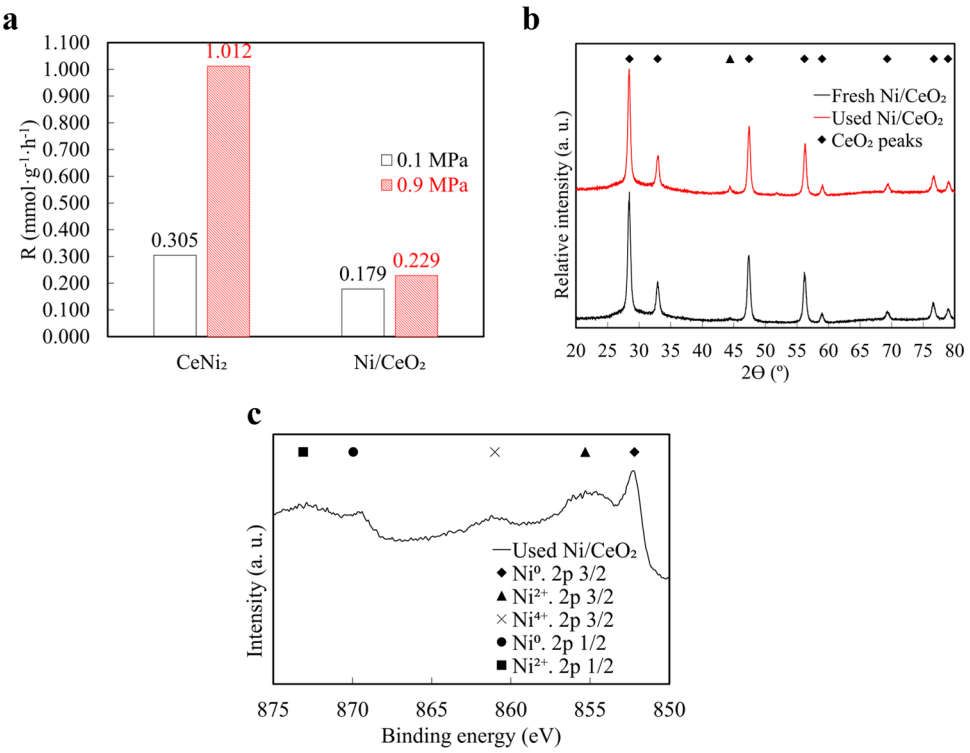

Figure 5. Ni/CeO_2 results and characterization. (a) Ammonia synthesis rates of $CeNi_2$ and Ni/CeO_2 at 0.1 and 0.9 MPa. Conditions: 400 °C, 36,000 mL g^{-1} h^{-1}, N_2/H_2 = 1:3, 0.1 g of the catalyst. (b) XRD crystal structure of fresh and used Ni/CeO_2. (c) Ni 2p XPS of the used Ni/CeO_2.

further suggesting that the strong difference in activity of both alloys originates from the formation of the CeN, which is absent in $CeNi_5$ (Figure 2b).

3.3. Role of Nickel in $CeNi_2$ and Bulk CeN Performance.

After the importance of the CeN surface layer formation was exposed, kinetic experiments were conducted for pure bulk CeN with no Ni loading. Despite having higher surface areas (2.78 vs 0.29 m^2 g^{-1}, Table S1), bulk CeN showed ammonia synthesis rates 1 order of magnitude lower than $CeNi_2$ at the same conditions (Figure 4a), thereby revealing the important role of Ni in the reaction. To further investigate these notable differences, additional experiments were carried out. The following kinetic parameters were obtained for bulk CeN—E_A: 72.1 kJ mol^{-1}, α: 0.806, γ: −0.444. This material showed a higher apparent activation energy and nitrogen reaction order (α) than $CeNi_2$, while both catalysts showed very similar hydrogen reaction orders (β). This could indicate that bulk CeN is less efficient than $CeNi_2$ in dissociating N_2 (the importance of this step in the kinetic mechanism is higher) and, eventually, to generate ammonia,[7,44,45] which was further confirmed by the less negative (closer to 0) ammonia order (γ). CeN maintained its crystal structure after the reaction (Figure 4b), revealing that the material is stable under the operation conditions used herein.

Previous studies revealed that CeN nanoparticles have a similar reaction mechanism than Ni/CeN nanoparticles.[16] For both catalysts, N_V vacancies generated over the surface of the nitride layer can dissociate N_2 and activate H_2 to produce ammonia simultaneously, leading to a competition between activated N_2 and H_2 species to occupy those vacancies, which act as second active sites. However, since the adsorption energy of H_2 on Ni is lower than that on N_V vacancies,[16] Ni can act as an additional active center for H_2 activation, leading to a higher number of nitrogen vacancy sites available for N_2 dissociation over CeN after Ni loading, greatly enhancing ammonia synthesis of the pure nitride.

In order to clarify the role of Ni on the global ammonia synthesis performance of $CeNi_2$, temperature-programmed desorption (TPD) analyses were conducted for CeN (both fresh and used samples) and $CeNi_2$ and $CeNi_5$. The H_2 TPD patterns of fresh CeN (Figure 4c) showed a peak at 300 °C, which can be ascribed to hydrogen associated with residual amounts of CeH_3 from the material synthesis process.[22] Regarding the used samples, no H_2 peaks were observed for $CeNi_5$, thereby revealing that this material cannot activate hydrogen as efficiently as CeN, which showed a noticeable peak at ca. 450 °C attributed to hydrogen species activated on N_V vacancies. Interestingly, compared to CeN, the onset temperature of this high-temperature hydrogen peak decreased to 380 °C for $CeNi_2$, thereby revealing a higher mobility of H_2 species over the N_V vacancy sites in this material. $CeNi_2$ also showed a low-temperature hydrogen peak at ca. 200 °C, which has been previously associated with Ni.[36] Similar results were obtained for $LaNi_5$ alloys with two hydrogen peaks at ca. 150 and 365 °C ascribed to Ni and LaN, respectively. Thus, Ni improves the ammonia synthesis reaction by promoting H_2 dissociation and therefore increasing the number of available surface N_V sites for N_2 dissociation, enhancing both N_2 dissociation and NH_3 generation. This mechanism is in good agreement with the mechanism exhibited by Ni/CeN.[16] However, regarding the differences in performance and kinetic mechanism between $CeNi_2$ and $CeNi_5$ shown in Section 3.1 and considering that nitrogen dissociation takes place mainly over the N_V sites for $CeNi_2$ after the preactivation stage, maximizing CeN presence over the catalyst surface seems to be an advantage of $CeNi_2$ alloy over previously reported Ni/CeN. The role of Ni was further confirmed by N_2 TPD (Figure 4d). The CeN sample used showed a predominant peak at 550−650 °C ascribed to the

release of N_2 from N_V sites. Remarkably, this peak shifted to significantly lower temperatures (480 °C) for the used $CeNi_2$, thereby suggesting a higher mobility of N_2 species over the N_V sites in the presence of Ni. The TPD peaks were integrated, and their normalized areas are shown in Table S2. The areas of both N_2 and H_2 peaks of the used $CeNi_2$ are 1 order of magnitude higher than those obtained for CeN and used $CeNi_5$. N 1s XPS patterns of both fresh and used pure CeN (Figure S2e) show that nitrogen is only in the form of CeN over the catalyst surface, unlike used $CeNi_2$, which is discussed in Section 3.1.

3.4. Role of Cerium Chemical State and Performance of Ni/CeO_2 Nanopowder. Once studied the roles of CeN (second active center for efficient N_2 dissociation) and Ni (promote the activation of hydrogen species),[16] we analyzed the role of Ce in the ammonia synthesis reaction. In order to study the chemical state of Ce and to verify Ce in a nitride form, the performance of $CeNi_2$ was compared to that of a simple catalyst of Ni supported on CeO_2. Thus, a Ni/CeO_2 (20 wt % of Ni) nanopowder catalyst was prepared and kinetic experiments were performed under the same conditions used for $CeNi_2$ (Section 3.1), with a previous preactivation stage at 500 °C for 2 h. The ammonia synthesis rates of Ni/CeO_2 and $CeNi_2$ are compared in Figure 5a. Despite the higher surface area of Ni/CeO_2 (30.35 vs 0.29 $m^2\ g^{-1}$ of $CeNi_2$, Table S1), this catalyst showed lower ammonia synthesis rates than $CeNi_2$. Furthermore, Ni/CeO_2 did not show a pressure effect as positive as expected (the rate only increased slightly at 0.9 MPa), considering the rest of the catalysts shown in this work.

The following kinetic parameters were obtained for Ni/CeO_2: E_A: 115.9 kJ mol^{-1}, α: 0.857, γ: −0.062. An apparent activation energy as high as 115.9 kJ^{-1} and an ammonia order (γ) close to zero are clear indicatives of a less efficient mechanism as compared to other catalysts reported in Sections 3.1 and 3.2. Furthermore, a negative hydrogen order (β) reveals a noticeable hydrogen poisoning, which can explain the poor effect of pressure effect on the synthesis rate for this catalyst.[7]

The XRD pattern of Ni/CeO_2 (Figure 5b) revealed no significant changes in the crystal structure after the reaction. Ni was present on an amorphous phase over the fresh catalyst, and this could indicate that nickelocene is not properly reduced after the initial prereduction stage after the solid-state reaction. Furthermore, a very small peak corresponding to Ni can be observed after the reaction, which could suggest that a certain amount of amorphous Ni remains after the synthesis procedure. Moreover, the catalyst preserved the CeO_2 crystal structure, with no peaks ascribed to reduced Ce_2O_3.[20,46] XPS analysis of the used Ni/CeO_2 (Figure 5c) revealed an uncomplete reduction of Ni species to Ni^0 during the preactivation stage or the experimental reaction, in contrast with CeN or $CeNi_x$ alloys. This incomplete reduction of Ni can also account for the hydrogen poisoning effect observed for Ni/CeO_2 ($\beta = -0.649$).

Considering the above results, the positive role of Ce in this reaction seems to be associated with this element forming a nitride phase, which serves as a second active center for N_2 dissociation. When Ce is in the form of oxide, the promotional effect in the ammonia synthesis reaction is rather limited, showing high activation energies and significant hydrogen poisoning, which results in lower synthesis rates and poorer pressure effects as compared to $CeNi_2$.

4. CONCLUSIONS

The importance of intermetallic RETM materials as effective ammonia synthesis catalysts is highlighted herein. This work demonstrates that $CeNi_2$ can efficiently dissociate nitrogen and produce ammonia by the spontaneous formation of a second active phase (crystalline CeN surface layer) generated in situ during the preactivation stage. The formation of this CeN phase is key for promoting the ammonia synthesis reaction, as demonstrated by the poor performance of $CeNi_5$, which, unlike $CeNi_2$, operated with no formation of CeN. Pure bulk CeN was found to be less efficient in dissociating N_2 and in forming NH_x species as compared to $CeNi_2$, thereby stressing the crucial role of Ni in this reaction. Ni was found to be key in promoting H_2 dissociation while increasing the number of N_V nitrogen vacancy sites available to dissociate N_2 and generate NH_3. Eventually, the importance of the Ce chemical state (oxide versus nitride) was highlighted herein. Ni/CeO_2 nanopowder showed a less efficient kinetic mechanism (higher activation energies, strong hydrogen poisoning, and poor affinity toward NH_x species) and lower synthesis rates than $CeNi_2$. The optimization of the Ce/Ni ratio and the operating conditions leading to the formation of the CeN layer over the $CeNi_x$ alloy can pave the way for efficient non-noble metal ammonia synthesis catalysts, which could also have particular scalable interest if they demonstrate to be air-stable.

Group, Department of Engineering, Universidad Loyola Andalucía, 41704 Dos Hermanas, Seville, Spain

Masayoshi Miyazaki − *MDX Research Center for Element Strategy, International Research Frontiers Initiative, Tokyo Institute of Technology, Yokohama 226-8503, Japan;* orcid.org/0000-0003-4343-1137

Author Contributions

This manuscript was written through contributions of all authors. All authors have given approval to the final version of the manuscript.

Funding

J.A.-C. would like to thank the University Loyola for the funds associated with the project "Design and screening of catalysts for the synthesis of ammonia at mild temperature and pressure conditions".

Notes

The authors declare no competing financial interest.

REFERENCES

(1) Food and Agriculture Organization of the United Nations. *World Fertilizer Trends and Outlook to 2022*; Rome, 2019.

(2) Smith, C.; Hill, A. K.; Torrente-Murciano, L. Current and Future Role of Haber-Bosch Ammonia in a Carbon-Free Energy Landscape. *Energy Environ. Sci.* **2020**, *13* (2), 331−344.

(3) Wang, Q.; Guo, J.; Chen, P. Recent Progress towards Mild-Condition Ammonia Synthesis. *J. Energy Chem.* **2019**, *36*, 25−36, DOI: 10.1016/j.jechem.2019.01.027.

(4) Rouwenhorst, K. H. R.; Van der Ham, A. G. J.; Lefferts, L. Beyond Haber-Bosch: The Renaissance of the Claude Process. *Int. J. Hydrogen Energy* **2021**, *46* (41), 21566−21579.

(5) 2020 Ammonfuel Report an Industrial View of Ammonia as a Marine Fuel, 2023. https://www.ocimf.org/?view=article&id=1289:2020-ammonfuel-report-an-industrial-view-of-ammonia-as-a-marine-fuel&catid=160. (accessed June 30, 2023).

(6) Ojelade, O. A.; Zaman, S. F. Ammonia Decomposition for Hydrogen Production: A Thermodynamic Study. *Chem. Pap.* **2021**, *75* (1), 57−65.

(7) Marakatti, V. S.; Gaigneaux, E. M. Recent Advances in Heterogeneous Catalysis for Ammonia Synthesis. *ChemCatChem* **2020**, *12*, 5838−5857, DOI: 10.1002/cctc.202001141.

(8) Humphreys, J.; Lan, R.; Tao, S. Development and Recent Progress on Ammonia Synthesis Catalysts for Haber−Bosch Process. *Adv. Energy Sustainability Res.* **2021**, *2* (1), No. 2000043.

(9) Li, L.; Zhang, T.; Zhou, Y.; Wang, X.; Au, C.-t.; Jiang, L. Review on Catalytic Roles of Rare Earth Elements in Ammonia Synthesis: Development and Perspective. *J. Rare Earths* **2022**, *11* (4), No. 2003723, DOI: 10.1016/j.jre.2021.06.014.

(10) Chang, F.; Gao, W.; Guo, J.; Chen, P. Emerging Materials and Methods toward Ammonia-Based Energy Storage and Conversion. *Adv. Mater.* **2021**, *33* (50), No. 2005721, DOI: 10.1002/adma.202005721.

(11) Hosono, H.; Kitano, M. Advances in Materials and Applications of Inorganic Electrides. *Chem. Rev.* **2021**, *121* (5), 3121−3185, DOI: 10.1021/acs.chemrev.0c01071.

(12) Reese, M.; Marquart, C.; Malmali, M.; Wagner, K.; Buchanan, E.; McCormick, A.; Cussler, E. L. Performance of a Small-Scale Haber Process. *Ind. Eng. Chem. Res.* **2016**, *55* (13), 3742−3750.

(13) Jacobsen, C. J. H.; Dahl, S.; Clausen, B. G. S.; Bahn, S.; Logadottir, A.; Nørskov, J. K. Catalyst Design by Interpolation in the Periodic Table: Bimetallic Ammonia Synthesis Catalysts. *J. Am. Chem. Soc.* **2001**, *123*, 8404−8405.

(14) Vojvodic, A.; Medford, A. J.; Studt, F.; Abild-Pedersen, F.; Khan, T. S.; Bligaard, T.; Nørskov, J. K. Exploring the Limits: A Low-Pressure, Low-Temperature Haber-Bosch Process. *Chem. Phys. Lett.* **2014**, *598*, 108−112.

(15) Wang, P.; Chang, F.; Gao, W.; Guo, J.; Wu, G.; He, T.; Chen, P. Breaking Scaling Relations to Achieve Low-Temperature Ammonia Synthesis through LiH-Mediated Nitrogen Transfer and Hydrogenation. *Nat. Chem.* **2017**, *9* (1), 64−70.

(16) Ye, T. N.; Park, S. W.; Lu, Y.; Li, J.; Sasase, M.; Kitano, M.; Hosono, H. Contribution of Nitrogen Vacancies to Ammonia Synthesis over Metal Nitride Catalysts. *J. Am. Chem. Soc.* **2020**, *142* (33), 14374−14383.

(17) Gong, Y.; Li, H.; Li, C.; Bao, X.; Hosono, H.; Wang, J. Insight into Rare-Earth-Incorporated Catalysts: The Chance for a More Efficient Ammonia Synthesis. *J. Adv. Ceram.* **2022**, *11* (10), 1499−1529.

(18) Lin, B.; Liu, Y.; Heng, L.; Wang, X.; Ni, J.; Lin, J.; Jiang, L. Morphology Effect of Ceria on the Catalytic Performances of Ru/CeO2 Catalysts for Ammonia Synthesis. *Ind. Eng. Chem. Res.* **2018**, *57* (28), 9127−9135.

(19) Sato, K.; Nagaoka, K. Boosting Ammonia Synthesis under Mild Reaction Conditions by Precise Control of the Basic Oxide−Ru Interface. *Chem. Lett.* **2021**, *50* (4), 687−696.

(20) Ma, Z.; Zhao, S.; Pei, X.; Xiong, X.; Hu, B. New Insights into the Support Morphology-Dependent Ammonia Synthesis Activity of Ru/CeO2 Catalysts. *Catal. Sci. Technol.* **2017**, *7* (1), 191−199.

(21) Wang, X.; Li, L.; Zhang, T.; Lin, B.; Ni, J.; Au, C. T.; Jiang, L. Strong Metal−Support Interactions of Co-Based Catalysts Facilitated by Dopamine for Highly Efficient Ammonia Synthesis: In Situ XPS and XAFS Spectroscopy Coupled with TPD Studies. *Chem. Commun.* **2019**, *55* (4), 474−477.

(22) Mizoguchi, H.; Okunaka, M.; Kitano, M.; Matsuishi, S.; Yokoyama, T.; Hosono, H. Hydride-Based Electride Material, LnH2 (Ln = La, Ce, or Y). *Inorg. Chem.* **2016**, *55* (17), 8833−8838, DOI: 10.1021/acs.inorgchem.6b01369.

(23) Ooya, K.; Li, J.; Fukui, K.; Iimura, S.; Nakao, T.; Ogasawara, K.; Sasase, M.; Abe, H.; Niwa, Y.; Kitano, M.; Hosono, H. Ruthenium Catalysts Promoted by Lanthanide Oxyhydrides with High Hydride-Ion Mobility for Low-Temperature Ammonia Synthesis. *Adv. Energy Mater.* **2021**, *11* (4), No. 2003723, DOI: 10.1002/aenm.202003723.

(24) Nakaya, Y.; Furukawa, S. Catalysis of Alloys: Classification, Principles, and Design for a Variety of Materials and Reactions. *Chem. Rev.* **2022**, *123* (9), 5859−5947, DOI: 10.1021/ACS.CHEMREV.2C00356/ASSET/IMAGES/MEDIUM/CR2C00356_0069.GIF.

(25) Croisé, C.; Alabd, K.; Tencé, S.; Gaudin, E.; Villesuzanne, A.; Courtois, X.; Bion, N.; Can, F. Influence of the Rare Earth (R) Element in Ru-Supported RScSi Electride-like Intermetallic Catalysts for Ammonia Synthesis at Low Pressure: Insight into NH3 Formation Mechanism. *ChemCatChem* **2023**, *15* (3), No. e202201172, DOI: 10.1002/cctc.202201172.

(26) Croisé, C.; Alabd, K.; Villesuzanne, A.; Can, F.; Courtois, X.; Gaudin, E.; Tencé, S.; Bion, N. Role of Hydride Ion within Ru/LaScSi and Ru/CeTiGe Catalysts for NH3 Synthesis: A Combination of DFT and Experimental Nitrogen Isotopic Exchange Studies. *Catal. Commun.* **2023**, *179*, No. 106689.

(27) Wu, J.; Li, J.; Gong, Y.; Kitano, M.; Inoshita, T.; Hosono, H. Intermetallic Electride Catalyst as a Platform for Ammonia Synthesis. *Angew. Chem., Int. Ed.* **2019**, *58* (3), 825−829.

(28) Li, J.; Wu, J.; Wang, H.; Lu, Y.; Ye, T.; Sasase, M.; Wu, X.; Kitano, M.; Inoshita, T.; Hosono, H. Acid-Durable Electride with Layered Ruthenium for Ammonia Synthesis: Boosting the Activity via Selective Etching. *Chem. Sci.* **2019**, *10* (22), 5712−5718.

(29) Gong, Y.; Wu, J.; Kitano, M.; Wang, J.; Ye, T. N.; Li, J.; Kobayashi, Y.; Kishida, K.; Abe, H.; Niwa, Y.; Yang, H.; Tada, T.; Hosono, H. Ternary Intermetallic LaCoSi as a Catalyst for N2 Activation. *Nat. Catal.* **2018**, *1* (3), 178−185.

(30) Latroche, M.; Percheron-Guégan, A. Structural and Thermodynamic Studies of Some Hydride Forming RM3-Type Compounds (R =

lanthanide, M = transition Metal). *J. Alloys Compd.* **2003**, *356*−*357*, 461−468.
(31) Joubert, J. M.; Paul-Boncour, V.; Cuevas, F.; Zhang, J.; Latroche, M. LaNi5 Related AB5 Compounds: Structure, Properties and Applications. *J. Alloys Compd.* **2021**, *862*, No. 158163.
(32) Santos, D. M. F.; Šljukić, B.; Amaral, L.; Macciò, D.; Saccone, A.; Sequeira, C. Nickel-Cerium Alloys for Borohydride Oxidation. *ECS Trans.* **2013**, *58* (1), 1893−1901.
(33) Tsukuda, R.; Ohhashi, S.; Xu, Y.; Nishimura, C.; Kameoka, S. Catalytic Hydrogenation of C2H2 over Amorphous CeNi2Hx and Crystalline CeNi2: Effects of Hydrogen-Induced Amorphization and Oxidation. *Mater. Trans.* **2022**, *63* (3), 343−350.
(34) Lushnikov, S. A. Desorption of Hydrogen from CeNi3 Intermetallic Hydrides. *Defect Diffus. Forum* **2010**, *297*−*301*, 35−39.
(35) Jiang, Y. F.; Liu, J. C.; Xu, C. Q.; Li, J.; Xiao, H. Breaking the Scaling Relations for Efficient N2-to-NH3 Conversion by a Bowl Active Site Design: Insight from LaRuSi and Isostructural Electrides. *Chin. J. Catal.* **2022**, *43* (8), 2183−2192.
(36) Ye, T. N.; Lu, Y.; Kobayashi, Y.; Li, J.; Park, S. W.; Sasase, M.; Kitano, M.; Hosono, H. Efficient Ammonia Synthesis over Phase-Separated Nickel-Based Intermetallic Catalysts. *J. Phys. Chem. C* **2020**, *124* (52), 28589−28595.
(37) Miyahara, S. I.; Sato, K.; Tsujimaru, K.; Wada, Y.; Ogura, Y.; Toriyama, T.; Yamamoto, T.; Matsumura, S.; Inazu, K.; Nagaoka, K. Co Nanoparticle Catalysts Encapsulated by BaO-La2O3Nanofractions for Efficient Ammonia Synthesis Under Mild Reaction Conditions. *ACS Omega* **2022**, *7* (28), 24452−24460.
(38) Kobayashi, Y.; Kitano, M.; Kawamura, S.; Yokoyama, T.; Hosono, H. Kinetic Evidence: The Rate-Determining Step for Ammonia Synthesis over Electride-Supported Ru Catalysts Is No Longer the Nitrogen Dissociation Step. *Catal. Sci. Technol.* **2017**, *7* (1), 47−50.
(39) Kitano, M.; Inoue, Y.; Yamazaki, Y.; Hayashi, F.; Kanbara, S.; Matsuishi, S.; Yokoyama, T.; Kim, S. W.; Hara, M.; Hosono, H. Ammonia Synthesis Using a Stable Electride as an Electron Donor and Reversible Hydrogen Store. *Nat. Chem.* **2012**, *4* (11), 934−940.
(40) Gong, Y.; Li, H.; Wu, J.; Song, X.; Yang, X.; Bao, X.; Han, X.; Kitano, M.; Wang, J.; Hosono, H. Unique Catalytic Mechanism for Ru-Loaded Ternary Intermetallic Electrides for Ammonia Synthesis. *J. Am. Chem. Soc.* **2022**, *144*, 8683−8692.
(41) Zheng, J.; Liao, F.; Wu, S.; Jones, G.; Chen, T.; Fellowes, J.; Sudmeier, T.; McPherson, I. J.; Wilkinson, I.; Tsang, S. C. E. Efficient Non-dissociative Activation of Dinitrogen to Ammonia over Lithium-Promoted Ruthenium Nanoparticles at Low Pressure. *Angew. Chem.* **2019**, *131* (48), 17496−17502.
(42) Miyahara, S.-i.; Sato, K.; Kawano, Y.; Imamura, K.; Ogura, Y.; Tsujimaru, K.; Nagaoka, K. Ammonia Synthesis over Lanthanoid Oxide−Supported Ruthenium Catalysts. *Catal. Today* **2021**, *376*, 36−40.
(43) Hiromoto, S.; Kano, K.; Suzuki, Y.; Asami, K.; Chiba, A.; Hanawa, T. Surface Characterization and Anodic Polarization of Nitrogen-Ion-Implanted Nickel-Free Co-Cr-Mo Alloy. *Mater. Trans.* **2005**, *46* (7), 1627−1632.
(44) Kitano, M.; Inoue, Y.; Ishikawa, H.; Yamagata, K.; Nakao, T.; Tada, T.; Matsuishi, S.; Yokoyama, T.; Hara, M.; Hosono, H. Essential Role of Hydride Ion in Ruthenium-Based Ammonia Synthesis Catalysts. *Chem. Sci.* **2016**, *7* (7), 4036−4043.
(45) Ye, T. N.; Park, S. W.; Lu, Y.; Li, J.; Sasase, M.; Kitano, M.; Tada, T.; Hosono, H. Vacancy-Enabled N2 Activation for Ammonia Synthesis on an Ni-Loaded Catalyst. *Nature* **2020**, *583* (7816), 391−395.
(46) Li, C.; Shi, Y.; Zhang, Z.; Ni, J.; Wang, X.; Lin, J.; Lin, B.; Jiang, L. Improving the Ammonia Synthesis Activity of Ru/CeO2 through Enhancement of the Metal−Support Interaction. *J. Energy Chem.* **2021**, *60*, 403−409.